

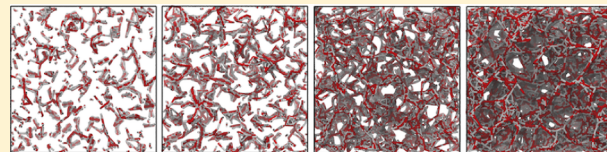
Effects of Water Concentration on the Structural and Diffusion Properties of Imidazolium-Based Ionic Liquid–Water Mixtures

Amir A. Niazi,* Brooks D. Rabideau, and Ahmed E. Ismail*

Aachener Verfahrenstechnik: Molecular Simulations and Transformations, Faculty of Mechanical Engineering, RWTH Aachen University, Schinkelstraße 2, 52062 Aachen, Germany

S Supporting Information

ABSTRACT: We have used molecular dynamics simulations to study the properties of three ionic liquid (IL)–water systems: 1-butyl-3-methylimidazolium chloride ([bmim]Cl), 1-ethyl-3-methylimidazolium acetate ([emim][Ac]), and 1,3-dimethylimidazolium dimethylphosphate ([dmim][DMP]). We observe the transition of those mixtures from pure IL to aqueous solution by analyzing the changes in important bulk properties (density) and structural and bonding properties (radial distribution functions, water clustering, hydrogen bonding, and cationic stacking) as well as dynamical properties (diffusion coefficients) at 12 different concentration samplings of each mixture, ranging from 0.0 to 99.95 mol % water. Our simulations revealed across all of the different structural, bonding, and dynamical properties major structural changes consistent with a transition from IL–water mixture to aqueous solution in all three ILs at water concentrations around 75 mol %. Among the structural changes observed were rapid increase in the frequency of hydrogen bonds, both water–water and water–anion. Similarly, at these critical concentrations, the water clusters formed begin to span the entire simulation box, rather than existing as isolated networks of molecules. At the same time, there is a sudden decrease in cationic stacking at the transition point, followed by a rapid increase near 90 mol % water. Finally, the diffusion coefficients of individual cations and anions show a rapid transition from rates consistent with diffusion in IL's to rates consistent with diffusion in water beginning at 75 mol % water. The location of this transition is consistent, for [bmim]Cl and [dmim][DMP], with the water concentration limit above which the ILs are unable to dissolve cellulose.



INTRODUCTION

Room-temperature ionic liquids (RTILs), which are salts that are liquids at standard temperature and pressure, provide desirable features such as very low vapor pressure, thermal stability, high ionic conductivity, nonflammability, and a large temperature range for which they remain liquid. Ionic liquids (ILs) and high-ionic-strength aqueous solutions of ILs are of significant commercial interest because of their potential as replacements for traditional organic solvents.^{1–3} One of the many advantages of ILs is the ability to tune physicochemical properties^{2,4–6} such as density, viscosity, conductivity, and hydrogen bonding by selecting appropriate cations, anions, and polar or nonpolar solvents.^{7–11}

RTILs are also attractive options as recyclable solvents for a range of different applications; one particular use that has been the subject of active investigation in recent years is as a solvent for pretreatment and dissolution of lignocellulosic biomass in the production of biofuels from biomass.^{12–14} Because the dissolution of cellulose will release the bound “structural” waters from the cellulose matrix, understanding the effect of water content on local ion–ion, ion–water, and water–water interactions at an atomistic scale is necessary for better understanding of the mechanism of catalytic cellulose dissolution in ILs.^{15–19}

Interactions between different types of ILs and water solvents are important because ILs can absorb a large amount of water

from the atmosphere.^{4,20–23} The solvation properties of ILs strongly depend on their miscibility with water and can be tailored in different ways. It has been reported for imidazolium-based ILs that hydrophobicity increases with the length of the cations’ alkyl tail and the size of anions.²⁴ Studies on the fundamental interactions of IL, water, and cellulose have provided guidance in optimizing processes for biomass pretreatment.²⁵

Recently, aqueous solutions of ILs have been the subject of numerous investigations, both experimental^{22,26–29} and computational.^{30–34} Cammarata et al.²³ studied the molecular state of water in ILs using IR spectroscopy. Additionally, various computational methods, such as molecular dynamics (MD) simulations,^{35–39} COSMO-RS,⁴⁰ and quantum mechanics calculations⁴¹ have been used to examine the interaction of different types of solutes in IL–water mixtures. Molecular dynamics simulations of the structure and dynamic properties of IL–water mixtures have been performed on 1,3-dimethylimidazolium chloride ([dmim]Cl) and 1,3-dimethylimidazolium hexafluorophosphate ([dmim][PF₆]) mixed with water.³³ Jiang et al.³⁰ studied the effect of water content on the nanostructural organization in 1-octyl-3-methylimidazolium ([omim][NO₃])–

Received: August 13, 2012

Revised: December 19, 2012

Published: January 9, 2013

water mixtures. Fang and Voth⁴² have analyzed the influence of both alkyl chain length and anion on the structure and dynamics of three ILs ($[\text{bmim}]^+ \text{BF}_6^-$, $[\text{omim}]^+ \text{BF}_4^-$ and $[\text{omim}]^+ \text{Cl}^-$) mixed in water. Recently, Hall and co-workers²⁹ have experimentally studied macroscopic and microscopic properties of $[\text{emim}]^+ \text{[Ac]}^-$ –water mixtures at different composition range from pure IL to pure water.

In this work, we perform molecular dynamics (MD) simulations to study the thermodynamic, structural, and mobility properties of mixtures of water with three imidazolium-based ILs: 1-butyl-3-methylimidazolium chloride ($[\text{bmim}]^+ \text{Cl}^-$), 1-ethyl-3-methylimidazolium acetate ($[\text{emim}]^+ \text{[Ac]}^-$), and 1,3-dimethylimidazolium dimethylphosphate ($[\text{dmim}]^+ \text{[DMP]}^-$). These ILs have been chosen because they have been found to be effective solvents for the dissolution of cellulosic biomass and because of their general commercial availability.^{40,43} In particular, we have focused on the effects and influence of varying water concentration on the structural and dynamical properties of these ILs. These ILs have been shown to be sensitive to the presence of water; beyond critical water concentrations, ILs are no longer able to dissolve cellulose.⁴³ We find that, in all three systems, there is a major shift in both structural and dynamic properties corresponding with water fractions of about 75 mol % or greater; these results are consistent with the experimental findings regarding the limits of cellulose dissolution for several of the ILs considered.

The remainder of this paper is organized as follows. In the next section, the atomistic models, force fields and simulation details are described. The Results and Discussion section provides analysis of our observations and calculated physical quantities, and the last section includes concluding remarks.

SIMULATION DETAILS

All MD simulations were performed using LAMMPS.⁴⁴ Figure 1 shows the molecular structure and atom-numbering scheme for the three different ILs simulated in this work. For each IL, we prepared a series of different systems, with the mole fraction of water varying from 0% (pure IL) to 99.95% (near-infinite dilution of the IL). Table 1 shows the mole, mass, and volume fractions for each of the 12 water concentrations studied.

The standard OPLS model has been used to represent the species in these simulations

$$\begin{aligned} U = & \sum_{\text{bonds}} k_r(r - r_0)^2 + \sum_{\text{angles}} k_\theta(\theta - \theta_0)^2 \\ & + \sum_{\text{dihedrals}} k_\phi[1 + \cos(n_0\varphi - \delta_0)] \\ & + \sum_{i < j} \left(4\epsilon_{ij} \left[\left(\frac{\sigma_{ij}}{r_{ij}} \right)^{12} - \left(\frac{\sigma_{ij}}{r_{ij}} \right)^6 \right] + \frac{q_i q_j}{r_{ij}} \right) \end{aligned} \quad (1)$$

where N is the number of atoms; q_i is the partial charge on atom i ; k_r , k_θ , and k_ϕ are coefficients for bond stretching, bending, and dihedrals; and σ_{ij} and ϵ_{ij} are the size and energy parameters in the Lennard-Jones potential. Force-field parameters for the $[\text{bmim}]$, $[\text{emim}]$, and $[\text{dmim}]$ cations as well as the chloride anion were taken from the work of Canongia Lopes et al.,⁴⁵ and for the $[\text{DMP}]$ and $[\text{Ac}]$ anions OPLS-AA force field parameters⁴⁶ have been applied. Water was simulated with the TIP3P water model.⁴⁷ All ionic liquid C–H bonds and water O–H bonds were held rigid using the SHAKE algorithm.⁴⁸

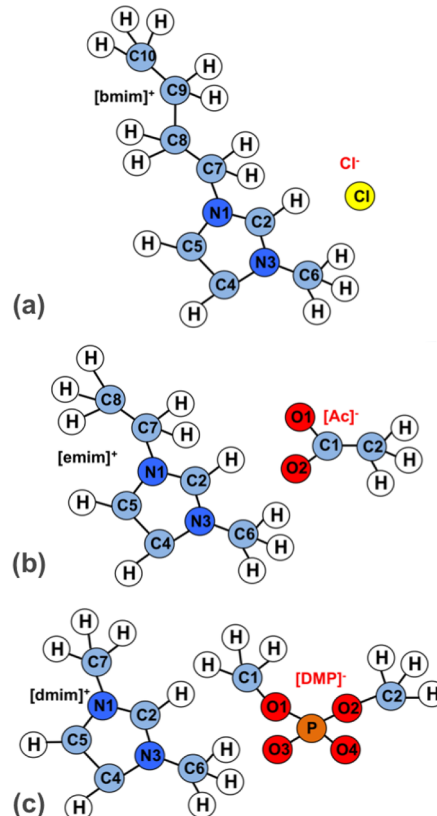


Figure 1. Structure and atom-numbering scheme of three different ILs: (a) 1-butyl-3-methylimidazolium chloride ($[\text{bmim}]^+ \text{Cl}^-$), (b) 1-ethyl-3-methylimidazolium acetate ($[\text{emim}]^+ \text{[Ac]}^-$), and (c) 1,3-dimethylimidazolium DMP ($[\text{dmim}]^+ \text{[DMP]}^-$).

For all systems, a cutoff distance of 12 Å was used for nonbonded interactions; the PPPM method⁴⁹ was used to treat long-range electrostatics, with an accuracy of one part in 10^4 and a 12 Å switching radius. The initial simulation box was a cube with sides of length 45 Å. To fix the system density, systems were equilibrated by running the system for 200 ps in the isothermal–isobaric (NPT) ensemble and the canonical ensemble (NVT) before beginning NVT production runs of 30 ns at 350 K with 1 fs time steps. For both the NVT and NPT simulations, a Nosé–Hoover thermostat with damping constant 100 fs⁻¹ was used; a Nosé–Hoover barostat with damping constant 500 fs⁻¹ was used to control the pressure. Coordinates of all atoms in the simulation box were written to an output file every 10 ps. Additionally, for each simulation, trajectories for the atoms of individual cations and anions were written into separate files every 0.5 ps. These single-ion trajectories were used to estimate the diffusivity of the IL as a function of water concentration.

Diffusion coefficients have been determined by fitting the mean square displacement (MSD) data using the Einstein transport equation

$$D = \frac{1}{6} \lim_{t \rightarrow \infty} \frac{d}{dt} \langle |r_i(t) - r_i(0)|^2 \rangle \quad (2)$$

where the angle brackets denote ensemble averages. To ensure that sufficient data is included in the averaging, multiple checkpoints from the trajectory of a single species or molecule were used as starting points in the calculation.

Table 1. Number of IL and Water Molecules Simulated for Different Water Mole Fractions

H ₂ O mole fraction (%)	no. of molecules		H ₂ O mass fraction (%)			H ₂ O volume fraction ^c (%)		
	IL	water	[dmim][DMP]	[emim][Ac]	[bmim]Cl	[dmim][DMP]	[emim][Ac]	[bmim]Cl
0 ^a	400	0	0	0	0	0	0	0
10	400	44	0.88	1.15	1.12	1.15	1.31	1.26
20	400	100	1.99	2.58	2.51	2.60	2.94	2.81
30	400	171	3.35	4.33	4.22	4.35	4.92	4.71
40	400	268	5.15	6.62	6.46	6.65	7.50	7.19
50	343	343	7.50	9.57	9.35	9.62	10.79	10.37
60	343	515	10.90	13.70	13.40	13.83	15.36	14.79
70	343	800	15.90	19.80	19.40	19.88	22.01	21.26
80	340	1360	24.30	29.70	29.20	29.64	32.56	31.63
90	150	1360	42.40	49.00	48.30	49.13	52.34	51.17
95	115	2200	60.80	66.90	66.40	67.05	69.79	68.91
99.95 ^b	1	2200	99.40	99.60	99.60	99.54	99.65	99.64

^aPure IL. ^bApproximation of the infinite-dilution limit. ^cVolume fractions have been calculated based on our simulation densities (g/cm³) at 350 K: $\rho_{[dmim][DMP]} = 1.24$, $\rho_{[emim][Ac]} = 1.08$, $\rho_{[bmim]Cl} = 1.06$, $\rho_{H_2O} = 0.945$.

RESULTS AND DISCUSSION

Density and Force Field Validation. To validate the mixing of force fields used to model the different pure ionic liquids, the density of each pure IL as a function of temperature was examined and compared against available experimental data.^{50,51} Figure 2 shows the comparison between simulated

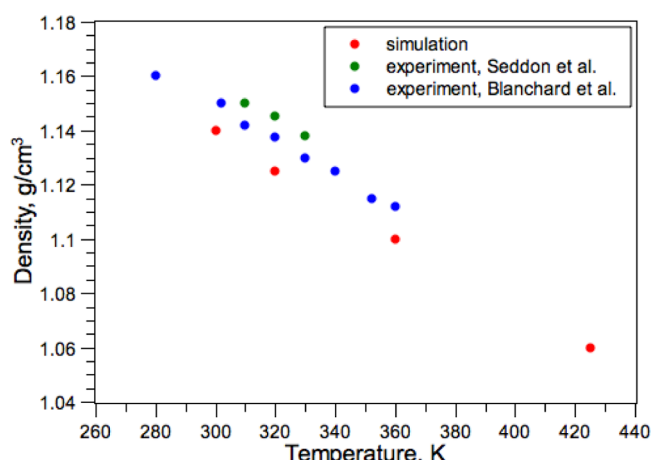


Figure 2. Density of [bmim]Cl ionic liquid calculated from MD simulations at 0.98 atm pressure and varying temperatures and compared against experimental data from Seddon and co-workers²⁴ and Blanchard and co-workers.⁵¹

and experimental densities at different temperatures calculated during 1 ns isothermal-isobaric MD simulations of [bmim]Cl. The deviations of simulated density values from experimental data reported by Seddon et al.²⁴ are in the range of 1–5%. Additionally, the same approximate slope for both simulation and experimental densities was also observed which indicates that the temperature variations are in good agreement. Similar results were obtained for [emim]Ac and [dmim][DMP].

In addition to densities, the excess molar volumes of the mixtures have been calculated and compared against available experimental data. Figure 3 shows our simulation results for the three IL–water mixtures at 350 K, as well as experimental data for [emim][Ac] at 300 K.²⁹ For all systems, the excess molar volume is relatively small, with a minimum at intermediate concentrations. Our results for [emim][Ac] are consistent with

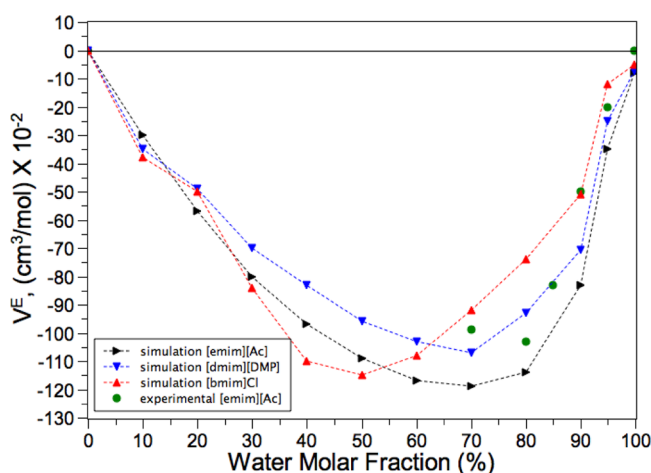


Figure 3. Simulated (triangular symbols) and experimental²⁹ (circular symbols) excess molar volumes of IL–water mixtures as a function of water content (mol %). All simulations are performed at 350 K and experimental values are reported at 300 K.

experimental trends,²⁹ which shows a minimum between 70 and 80 mol % water and comparable magnitudes for the excess molar volume, and with other simulation results, which show a minimum in the excess molar volume of approximately $-1.0 \text{ cm}^3/\text{mol}$.⁵²

Structural and Bonding Properties. Molecular Structure and Influence of Water. To determine the effect of water molecules on the structural properties of the three IL systems, we calculated the radial distribution functions (RDFs) for mixtures with water at the concentrations given in Table 1. For all three ILs, the C2 carbon atom of the imidazolium ring is selected to represent the cation, while water molecules are represented by their oxygen atoms. For the polyatomic anions, the carboxylate carbon (C1) of acetate and the phosphorus atom of dimethylphosphate, as shown in Figure 1, were used as reference atoms.

Figure 4 shows RDFs for those binary mixtures calculated from MD simulation of [bmim]Cl with water molar fractions of 20, 40, 60, 80, and 90%. For clarity, results at other concentrations have been omitted, as they were similar to those presented here. For the [bmim]Cl–water system, the strongest association between cations and anions is observed at

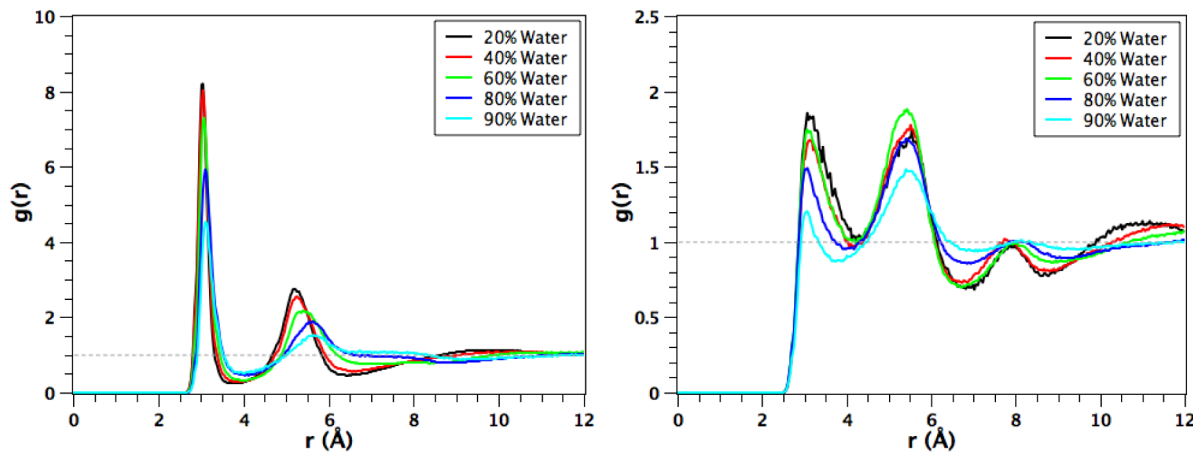


Figure 4. Radial distribution functions of cations with (left) anions and (right) water molecules in $[\text{bmim}]\text{Cl}$ -water mixtures.

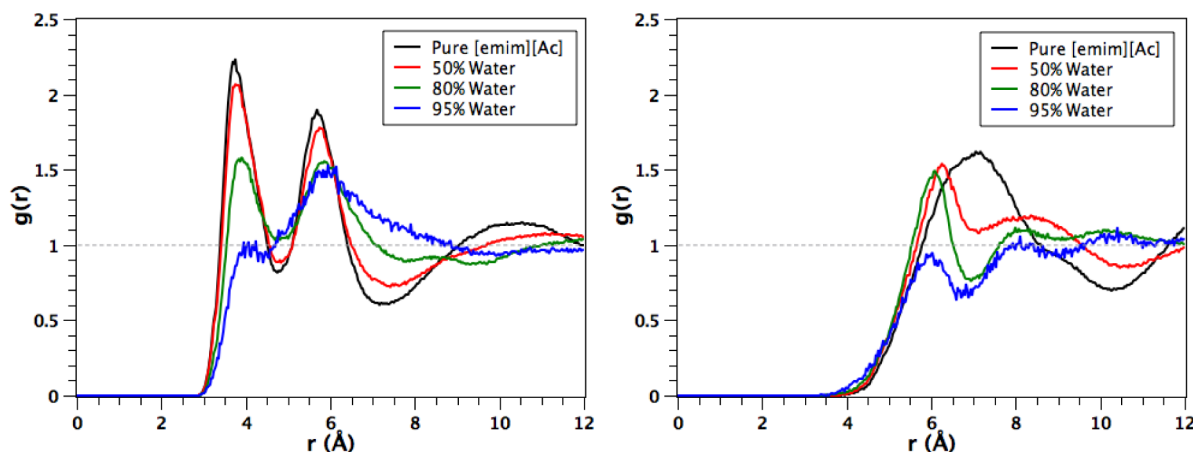


Figure 5. Radial distribution functions of (left) cation-anion and (right) anion-anion pairs calculated for different water molar fractions in $[\text{emim}]\text{[Ac]}$ -water mixtures.

20% water molar fraction, with a very sharp first peak centered at around 3.8 Å. Similar behavior is observed for cation–water interactions, with a peak at 3.2 Å, although the peak is broader and less pronounced than the cation–anion peak. These results indicate that the spatial correlation of cations with anions and water molecules at high (90%) water concentrations is weaker than those observed at low concentrations (20%).

Also worth noting is the presence of a secondary peak at about 5.5 Å in the cation–anion RDF and secondary and tertiary peaks at 3.2 and 5.5 Å in the cation–water RDF. While these peaks are visible at lower concentrations, they are “smoothed out” at 80% and higher water concentrations. These results suggest that at very high water concentrations the chloride ions and water oxygens form a shell around the central $[\text{bmim}]^+$ cation and the water hydrogens.

Figure 5 shows interactions between cation–anion and anion–anion pairs of $[\text{emim}]\text{[Ac]}$ computed for pure IL and for water mole fractions of 50, 80, and 95%. For cation–anion interactions, the strongest clustering of ion pairs in the pure IL occurs at around 3.8 Å, followed by a second sharp peak at around 5.8 Å. As the water mole fraction is increased to 80%, the magnitude of the peaks monotonically decreases, indicating disruption of cation–anion networks by water molecules. These results for cation–anion interactions are in agreement with observations of Liu et al.²⁵ for the $[\text{emim}]\text{[Ac]}$ -water system. For anion–anion interactions, the addition of water

molecules leads to an even greater change: for the pure IL, there is a single $g(r)$ peak for the range between 5.0 and 8.5 Å; the addition of water leads to the splitting of this peak into two separate shells, centered around 6.0 and 8.0 Å. As the water concentration increases, the peak around 6.0 Å decreases in size relative to the 8.0 Å peak, consistent with the formation of solvation shells around both anions.

Radial distribution functions for interactions between cations, anions, and water molecules for six different water mole fractions (0, 10, 30, 50, 80, and 95 mol %) in $[\text{dmim}]\text{[DMP]}$ are shown in Figure 6. For water mole fractions up to 50%, there are peaks in the anion–anion $g(r)$ at about 7.0 and 13.5 Å. However, at concentrations of 80% and higher, it can be seen that anion–anion pairs are uniformly distributed, and the peak at 13.5 Å disappears as water is added. The radial distribution functions also suggest that, unlike anion–anion pairs, cation–anion pairs weakly interact with each other. In addition, there is a corresponding sharpening of the cation–anion peak at approximately 4.0 Å, which indicates that the $[\text{dmim}]^+ - [\text{DMP}]^-$ pairs tend to aggregate more closely as water concentration increases. Comparing the behavior of the two peaks also shows that the first peak goes through a maximum at intermediate water concentrations, while the second peak slowly decreases. The behavior of the cation–water distribution function is much more complicated: for water concentrations above 50 mol %, there are sharp reductions in the $g(r)$ peaks at

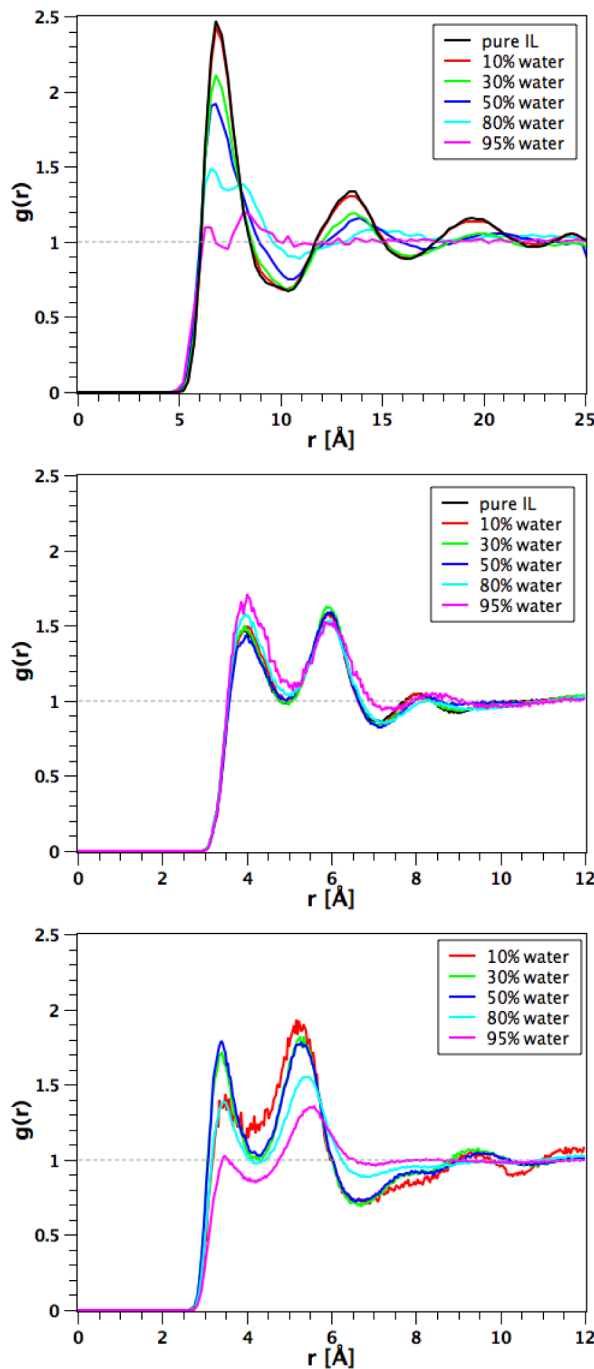


Figure 6. Influence of water concentration on radial distribution functions of $[\text{dmim}][\text{DMP}]$ -water mixtures: (top) anion-anion, (middle) cation-anion and (bottom) cation-water pairs.

both 3.5 and 5.5 Å. This result suggests that there is a tendency toward solvation for low and medium water concentrations, but at higher concentrations, the trend is toward formation of an essentially random solution, except with aggregated $[\text{dmim}]^+ - [\text{DMP}]^-$ pairs instead of lone ions.

Hydrogen-Bond Interactions. We have examined the formation of hydrogen bonds between water–water, water–cation, water–anion, and cation–anion pairs at different water concentrations. On the basis of previous geometric definitions of hydrogen bonds,^{53,54} we consider a hydrogen bond to exist if the radial distance between the labeled hydrogen and the acceptor atom is equal to or shorter than 2.45 Å and the angle

of the acceptor–donor hydrogen is less than 30° (see Figure 7). For this angle, acceptor/donor atoms correspond to water

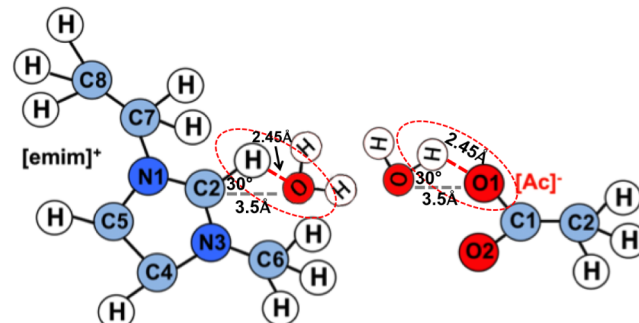


Figure 7. Geometric criteria used in this work for the calculation of number of hydrogen bonds formed between (left) water–cation and (right) water–anion pairs. Here, $[\text{emim}][\text{Ac}]$ is chosen as a representative for the other ILs.

oxygens/acidic aromatic carbons in water–cation interactions and anion oxygens/water oxygen in water–anion interactions, respectively. The latter condition requires the distance between acceptor and donor atoms to be less than 3.5 Å.

The results of our calculations suggest that, among four different pairs mentioned above, water–water and water–anion pairs have a greater tendency to form hydrogen bonds than the other two water–cation and cation–anion pairs. Figure 8 shows

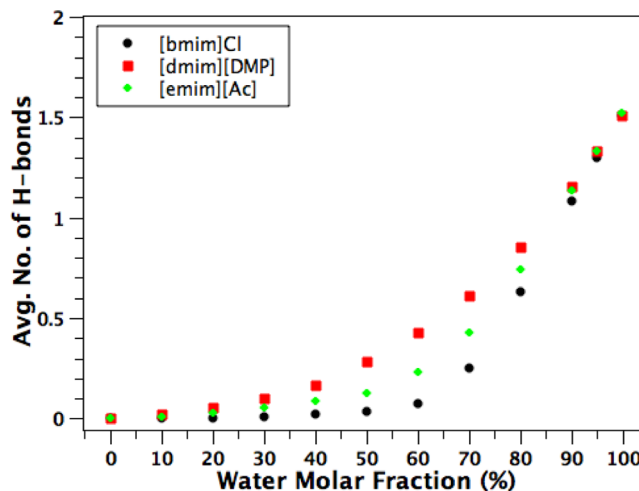


Figure 8. Average number of water–water hydrogen bonds per water molecule formed at different water molar fractions.

the average number of water–water hydrogen bonds in the three IL–water mixtures. For each system, the average number of water–water hydrogen bonds per water molecule increases essentially monotonically with water concentration. It can be seen that, at very low and very high water contents, all three systems have almost the same number of water–water hydrogen bonds, while at intermediate water contents, especially around 65 mol %, there are clear differences in the average number of hydrogen bonds. In this concentration range, $[\text{dmim}][\text{DMP}]$ has the most and $[\text{bmim}]\text{Cl}$ has the fewest hydrogen bonds, consistent with the clustering of $[\text{dmim}][\text{DMP}]$ observed at intermediate concentrations.

According to the criteria we have employed in this work, for water–anion pairs we have considered water oxygens as donors

and the anion oxygens (and chloride atom) of anions as acceptors. The number of water–anion hydrogen bonds are shown in Figure 9 on a per-anion basis. These bonds are about

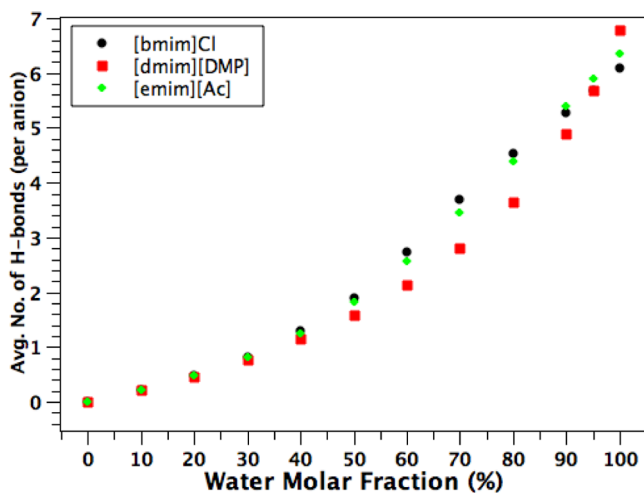


Figure 9. Average number of water–anion hydrogen bonds per anion molecule as a function of water molar fraction.

4 times more common than water–water hydrogen bonds. It can be seen that individual anions form increasing numbers of hydrogen bonds as the water concentration increases and only at low water concentrations do all three systems have the same number of hydrogen bonds. As separation starts at about 50% this time, unlike in water–water pairs, [bmim]Cl shows the largest number of hydrogen bonds. This can be explained by easier accessibility of monatomic Cl anions than other two polyatomic anions. Although the dimethylphosphate ion has twice as many oxygen ions as the acetate ion, the presence of the methyl groups around two of the oxygens partially restricts their ability to form hydrogen bonds at intermediate concentrations.

Cationic Stacking Interactions. Another interesting feature of imidazolium-based ILs is the “stacking” of cations through alignment of the imidazolium rings. To examine the possibility of π -orbital stacking in neighboring imidazolium rings, we consider two different geometries: parallel face–face and parallel displaced.⁵⁵ On the basis of these geometries, for each pair of cations i and j , we define R as the distance between the geometric centers of two imidazolium rings and \mathbf{n}_i and \mathbf{n}_j as the normal vectors to the planes of rings i and j , respectively. Figure 10 shows a schematic view of the geometric criteria: θ is the angle between the normal vector and the center-to-center

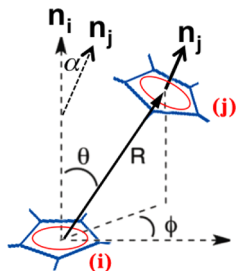


Figure 10. Schematic representation of the geometry of two imidazolium rings i and j with the normal vectors \mathbf{n}_i and \mathbf{n}_j and center–center separation vector R .

vector R , ϕ is the rotation angle of the rings with respect to each other, and α is the angle defined by the dot product of the normal vectors \mathbf{n}_i and \mathbf{n}_j . We can distinguish two different geometries: parallel face–face, with $\alpha = \theta = 0$, and parallel displaced, with $\alpha = 0$ and $0 < \theta < 60^\circ$.

We consider here parallel face–face and parallel displaced geometries, and refer to them together as parallel stacking. In each system, the maximum separation distance R^* of individual cation pairs counted as “stacked” was taken to be 4.5 Å consistent with similar measurements and studies.⁵⁵ Figure 11

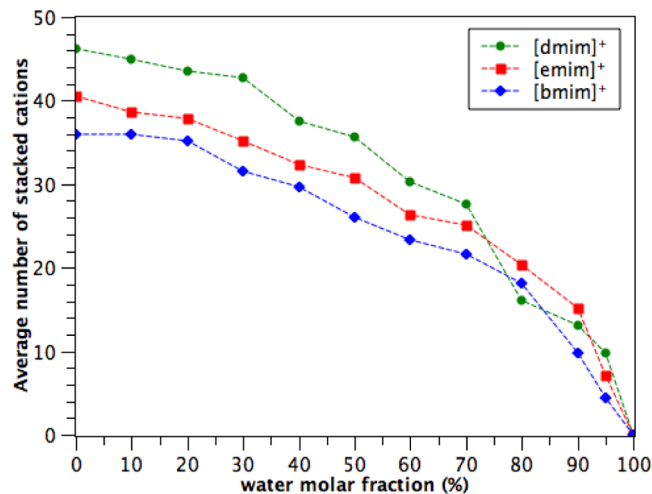


Figure 11. Average number of stacked cations as a function of water mole fraction.

shows the average number of stacked cations for all three systems at the different water molar concentrations calculated based on the parameters described above. It can be seen that, for all mixtures, the number of stacked cations decreases with increasing water concentration. This is consistent with the interspersion of water molecules between the rings, which can push the rings sufficiently far away from one another that stacking is no longer possible. Of the three ILs considered, $[\text{dmim}]^+$, the smallest of the three cations, exhibits greater stacking than the $[\text{bmim}]^+$ and $[\text{emim}]^+$; the additional steric hindrance caused by the longer tails of the $[\text{bmim}]^+$ and $[\text{emim}]^+$ cations make alignment of the rings more difficult.

Additionally, Figure 12 shows the percentage of stacked cations as a function of water concentration. For low to medium water concentrations, the percentage of stacked cations depends only weakly on the amount of water present; however, there is still a slight decrease caused by the water molecules interpenetrating between the cations. Above 70% water, we see that the variations are much more extreme, with all three cations going through a pronounced minimum at 80%. At 90% water, there is a sharp increase, which suggests that the IL shows an increased tendency to cluster when it is effectively “dissolved” in water, such that the formation of stacked rings is an energetically favorable configuration. However, such interactions remain relatively infrequent, as the percentage of cations exhibiting stacking conditions is only in the range of about 6–10%. Further experimental or simulation work on stacking in aqueous mixtures and solutions is necessary to verify this hypothesis. Additional information about histograms of averaged number of cations per frame as a function of center–center distances (R) for two selected systems as well as cation–

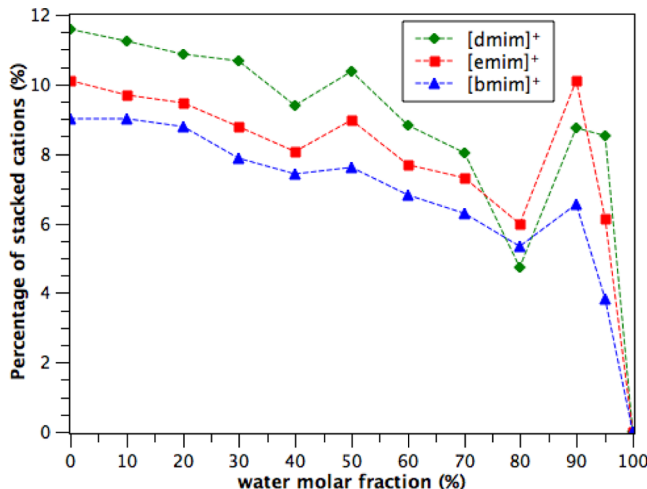


Figure 12. Percentage of stacked cations as a function of water mole fraction.

cation RDFs at different water concentrations can be found in the Supporting Information.

Water Clustering. To further quantify the extent of the structural changes occurring as water concentration increases, we have also measured the formation of water clusters and networks inside the ILs. For this calculation, we focused on the behavior of water molecules during the last 2 ns of the simulations. A given water molecule was represented by its center of mass; another water molecule was considered part of the same cluster if it was located within $2^{1/6}\sigma_{\text{OO}}$ of another water molecule that was already part of the cluster.

Figure 13 shows the average size of the biggest water clusters formed during the last 2 ns of each simulation as a function of

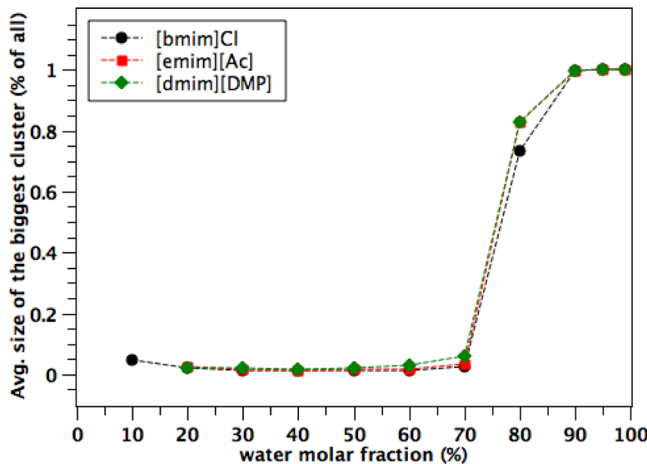


Figure 13. Average size of the biggest water clusters formed at different water concentrations.

water concentration. Here, the size of a cluster is the number of interconnected water molecules. For each of the ILs, the number of water clusters increases slowly up to about 60% water. At concentrations of 70% and above, there is a significant jump both in the size of the clusters, as well as the rate of growth with respect to increasing water concentration. It can be observed that, at low concentrations, water molecules are isolated and clearly separated from each other because of their smaller cluster sizes (see water molar fractions smaller than

70% in Figure 13). However, at about 70 mol % water, all systems experience a transition, in terms of cluster size, from small to very large clusters.

The transition in cluster size can be clearly seen from the simulation snapshots shown in Figure 14, where tiny and independent globules of water inside [emim][Ac]-water mixture at 60 mol % move toward formation of an extensive network throughout the simulation cell at 90 mol % (Figure 14d). It is also worth remarking here that analysis of morphologies of water clusters suggest that, at low water contents, H₂O molecules tend to form linear chains (Figure 14a) while as the system grows many small aggregates form a few but large honeycombed networks (Figure 14d). These observations of water clusters are in good agreement with previous studies of similar and other IL-water mixtures.^{33,56,57}

In addition to the size of the biggest clusters, we also calculated the average number of nearest neighbors of the biggest water clusters; the results are shown in Figure 15. It can be seen from this figure that, at concentrations higher than 80%, each water molecule begins to have on average more than 2.5 water neighbors, which again suggests that, by addition of water molecules to the system, clusters shift from small and isolated groups to large continuous networks. This analysis provides further evidence supporting the hypothesis that ordering of molecules is at its maximum for the fully solvated IL, with a transition to an aqueous solution of IL at higher concentrations.

Diffusion Coefficients. To understand the influence of water content on the dynamical properties of IL-water mixtures, the diffusion coefficients of cations and anions of the three ILs have been determined. The diffusion coefficients for the cations, shown in Figure 16, indicate that the diffusion constant increases nearly monotonically with water concentration, as expected, since water molecules can be displaced more readily than the IL.

The diffusion constants for all three ILs are approximately constant for water concentrations below 70 mol %. Above this value, however, two trends are of note. First, there is a substantial increase in the diffusion constant as water concentration increases. In addition, we see a separation in the magnitudes of the diffusion constants, up to 80%, consistent with the fact that smaller cations move faster than their heavier counterparts. The rapid increase in the diffusion constant and “crossover” behavior at approximately 85 mol % suggests that the system changes from a water-IL mixture to an aqueous IL solution. It can further be seen from Figure 17 that anions show similar diffusion behavior to that of the cations, except that differences in the magnitudes of the diffusion coefficients happen only above 90 mol %. At low concentrations, the size of the cation appears to be the limiting factor in the anion diffusion rate, as chloride ions appear to diffuse more slowly than the much larger dimethylphosphate ions at 10 mol % water. At high concentrations, the size of the individual ions controls the diffusion rate, as chloride diffuses significantly faster than either acetate or dimethylphosphate at near-infinite dilution.

Furthermore, for [dmim][dmp], there appears to be a slight downturn in the diffusivity between 80 and 90 mol %. This dropoff can be associated with both the structural changes discussed in the previous section and possible hysteresis behavior: there may be a range of concentrations for which the system can exist either as an IL-water mixture or as an aqueous IL solution. The results shown in Figures 16 and 17 are also

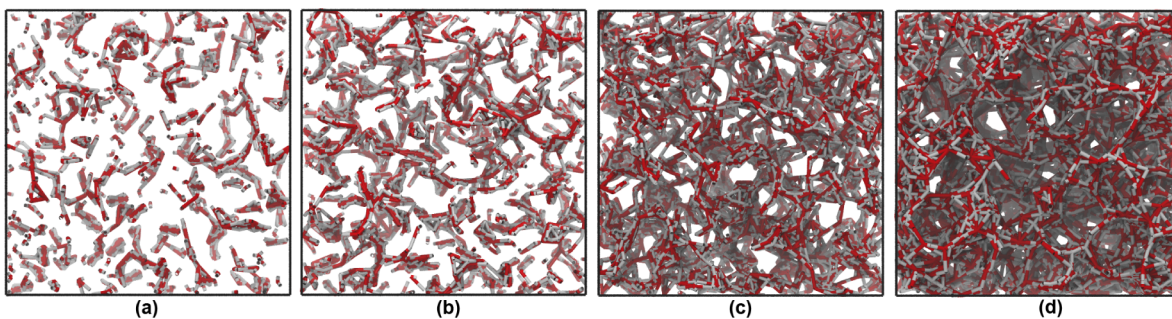


Figure 14. Simulation box snapshots of the water clusters formed in [emim][Ac] at (a) 60%, (b) 70%, (c) 80%, and (d) 90% water mole fractions.

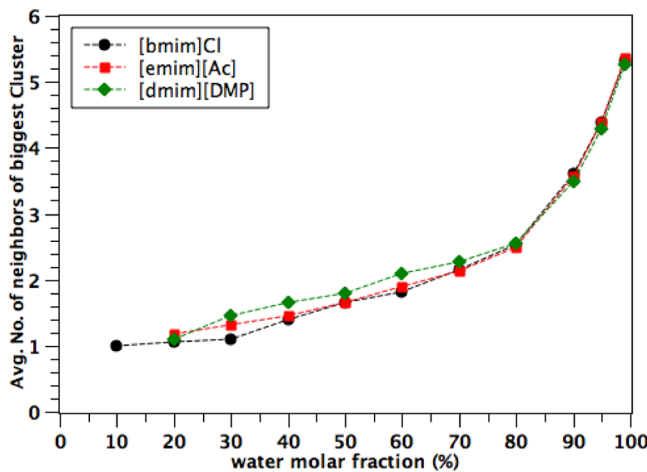


Figure 15. Average number of nearest neighbors of the biggest clusters of water molecules formed at different water concentrations.

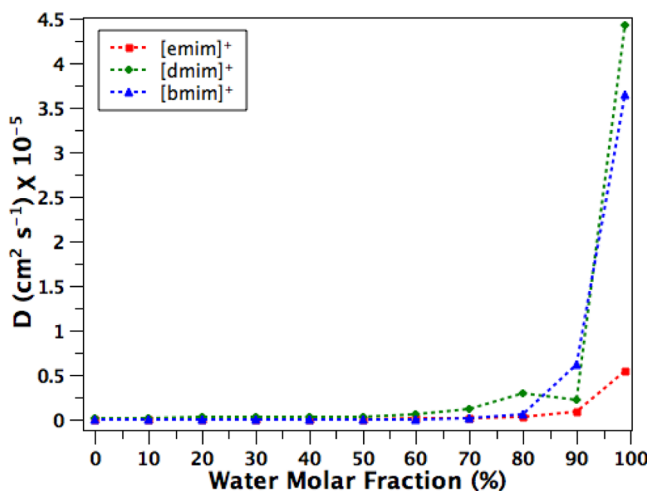


Figure 16. Diffusion coefficients of three different cations as a function of water molar fraction calculated from 30 ns MD simulations.

presented in tabular form and can be found in Supporting Information.

We have also calculated diffusion coefficients for water molecules moving among the different ILs, as well as their autodiffusion coefficients. Table 2 shows diffusion coefficients of one water molecule calculated from 30 ns simulations at 0.25%, 99.95%, and 100% water molar fractions, respectively. At all concentrations, diffusivity tends to decrease with increasing side-chain length.

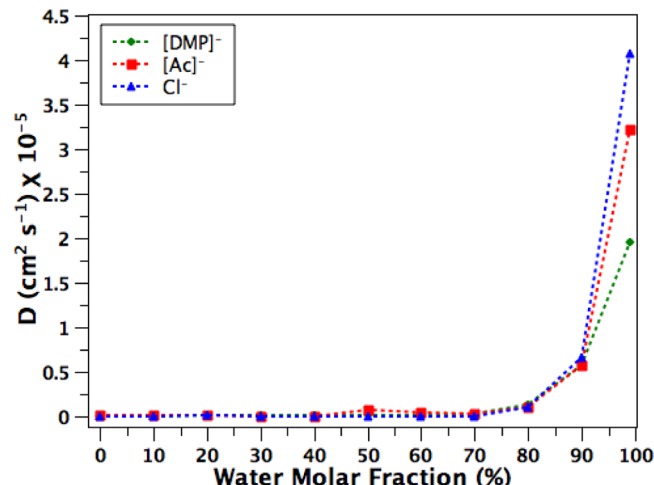


Figure 17. Diffusion coefficients of three different anions as a function of water molar fraction calculated from 30 ns MD simulation.

Table 2. Diffusion Coefficient of Water at 350 K Calculated for Pure Water System (100%), at near-Infinite Dilution of IL in Water (99.95%) and at near-Infinite Dilution of Water in IL (0.25%)

system	water (mol %)	diffusivity $D \times 10^{-5}$ (cm ² /s)
bmim-Cl/water	0.25	0.32
emim-Ac/water	0.25	0.81
dmim-DMP/water	0.25	1.23
bmim-Cl/water	99.95	7.90
emim-Ac/water	99.95	8.27
dmim-DMP/water	99.95	8.44
pure water	100	8.51

All of the results for diffusivity of IL-water systems show reasonable agreement with other studies on similar systems or at least on similar components. The comparisons between the results of this work and some available references are summarized in Table 3. It should be noted that the diffusion coefficients reported here are for systems with fixed charges, as polarizable force fields have not been considered.

Of note in the table are comparisons with the work of Kowsari and co-workers,³⁸ who calculated the diffusion coefficient of approximately 6.6×10^{-8} cm²/s for [bmim]Cl at 380 K, which is roughly 4 times higher than the values we have calculated at 350 K (1.69×10^{-8} cm²/s). In addition to the obvious changes as a result of the temperature increase, this difference may also be the result of Kowsari et al. using MSD data for time less than 150 ps for fitting of the diffusion coefficients. We further note that all of the force fields

Table 3. Diffusion Coefficients of IL Cations and Anions Simulated in This Work and in the Recent Literature

	diffusion coefficients (in $10^{-8} \text{ cm}^2 \text{ s}^{-1}$) of pure ILs ^a							
	298.15 K	300 K	343.2 K	350 K	380 K	400 K	423 K	420 K
[dmim]⁺[dmp]⁻	—	—	—	10.6 ^b	—	41.1 ^b	—	—
[emim]⁺[Ac]⁻	—	5.45 ^e	—	8.85 ^b	—	39.9 ^b	—	93.7 ^e
[bmim]⁺[Cl]⁻	—	—	—	1.69 ^b	6.8 ^c	7.2 ^c	—	—
[dmim]⁺[dmp]⁻	—	—	—	8.24 ^b	—	4.95 ^b	—	—
[emim]⁺[Ac]⁻	—	4.1 ^e	—	12.0 ^b	—	39.1 ^b	—	93.3 ^e
[bmim]⁺[Cl]⁻	—	—	—	4.66 ^b	6.4 ^c	7.5 ^c	—	—
[bmim]⁺[PF₆]⁻	9.7 ^f	—	12.1 ^f	—	—	—	—	—
[dmim]⁺[Cl]⁻	—	—	—	—	—	—	27.0 ^c	—
[dmim]⁺[Cl]⁻	—	—	—	—	—	—	18.5 ^c	—
[hmim]⁺[Cl]⁻	2.0 ^d	—	—	—	—	—	—	—

^aDiffusion coefficients are for the ion indicated in bold. ^bOur work. ^cKowsari et al.³⁸ ^dMendez-Morales et al.⁵⁹ ^eLiu et al.³⁵ ^fMorrow and Maginn.⁶⁰

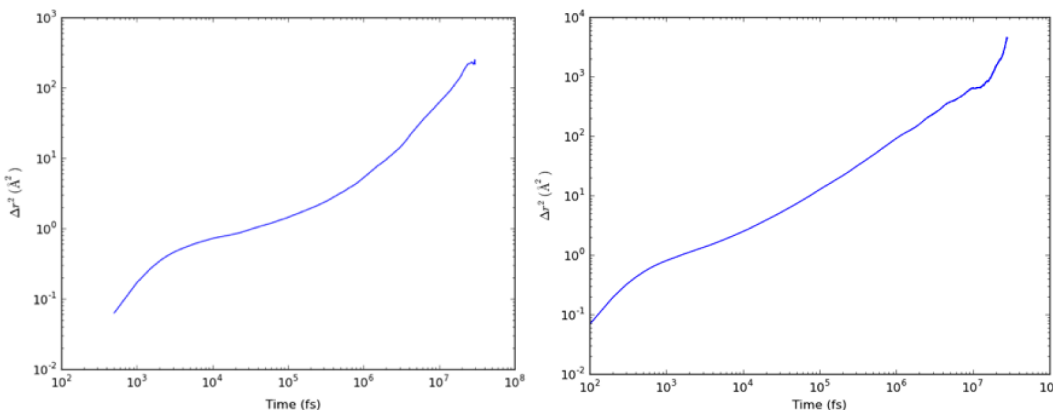


Figure 18. Mean square displacement vs time for [emim] cations with water concentrations of (left) 0 mol % water and (right) 80 mol % water. Three different anions as a function of water molar fraction calculated from 30 ns MD simulation of three different mixtures of [bmim]Cl, [emim][Ac], and [dmim][DMP] ionic liquids in water.

considered in this work are nonpolarizable; this would of course tend to lead to estimates of diffusion coefficients which are somewhat larger than one would expect from polarizable force fields of the same materials.

Another comparison of interest is with the work of del Pópolo and Voth³⁷ as well as that of Méndez-Morales and co-workers,⁵⁸ who both showed evidence of complex nonlinear diffusion in ILs and dilute mixtures. As seen in Figure 18, our work also shows evidence of such behavior for low concentrations, with a linear regime only established for pure [emim] cations at times longer than approximately 1 ns; at shorter times, we see evidence of a “shelf” such as those proposed by the previous studies.^{37,58} This “shelf” disappears at high water concentrations, suggesting that the behavior is not that of a mixture dominated by the ionic liquid components, but instead having the characteristics of an aqueous solution with the IL acting as solute. While the noise in the plots at the end of the graph is due to a lack of precision in the data resulting from a small number of available measurements, such data has not excluded from the fit of the diffusion coefficients, which are only applied to the linear region. We note that the present studies take into account 30 ns of simulation data in measuring the diffusion coefficients, while the previous studies were between 0.5 and 2 ns in length.

More details on diffusion coefficient calculations, including single-cation and single-anion log–log MSD plots at one selected concentration, are available in the Supporting Information.

CONCLUSIONS

Results of MD simulations of the [bmim]Cl–water, [emim][Ac]–water, and [dmim][DMP]–water mixtures at 350 K for a range of water concentrations have been reported to study the effect of water content on the structure and dynamics of these systems. We find that in all three systems, at low to intermediate water concentrations, the IL behavior largely tracks those of the pure ILs, particularly with respect to their dynamic properties ranging up to approximately 70 mol %. As the water content increases, there appears to be greater solvation around the IL cations and anions; beyond the 70 mol % range, the system transforms into an aqueous solution with the IL as solute. This conclusion is also supported by data from hydrogen bonding, water clustering, and diffusivity calculations.

For all three systems, we have also observed that during sufficiently long simulations, approximately beyond 70% water content, the diffusivity of both cations and anions begin a rapid increase with respect to concentration, corresponding to the transition to an aqueous solution. Addition of water molecules also reduces the strength of cationic stacking interactions by occupying the space above and below the imidazolium rings, thereby reducing the likelihood of forming stacked cations. Taken together, these findings support experimental evidence suggesting that solutions of ILs containing more than approximately 70 mol % water are unable to dissolve cellulose,⁴³ consistent with a transformation in the character of the system from an IL–water mixture to an aqueous solution.

Further work in this area could address how to separate the effects of the cation and anion in determining the structure and behavior of the ILs in solution; with the current set of ILs, there are no common cations or anions between the different mixtures, making the elucidation of trends more challenging. A combinatorial investigation of these systems would allow for the exploration of additional effects, such as the odd–even chain length behavior in the ability of imidazolium-based ILs to dissolve cellulose.⁶¹

■ ASSOCIATED CONTENT

Supporting Information

RDF's for the various cation–cation pairs, selected MSD plots for the cations and anions, and histograms for the cationic stacking calculations have been included. This material is available free of charge via the Internet at <http://pubs.acs.org>.

■ AUTHOR INFORMATION

Corresponding Author

*E-mail: niazi@aices.rwth-aachen.de (A.A.N.); aei@alum.mit.edu (A.E.I.).

Notes

The authors declare no competing financial interest.

■ ACKNOWLEDGMENTS

The authors thank Jörn Viell for useful discussions in the preparation of this manuscript. This work was performed as part of the Cluster of Excellence “Tailor-Made Fuels from Biomass,” which is funded by the Excellence Initiative by the German federal and state governments to promote science and research at German universities.

■ REFERENCES

- (1) Rogers, R. D.; Seddon, K. R. *Science* **2003**, *302*, 792.
- (2) Wasserscheid, P.; Keim, W. A. *Angew. Chem., Int. Ed.* **2000**, *39*, 3772.
- (3) Welton, T. *Chem. Rev.* **1999**, *99*, 2071–2084.
- (4) Wasserscheid, P., Welton, T., Eds. *Ionic Liquids in Synthesis*; Wiley-VCH: Weinheim, Germany, 2002.
- (5) Rogers, R. D., Seddon, K. R., Eds. *Ionic Liquids III A: Fundamentals, Progress, Challenges, and Opportunities and Properties and Structure*; American Chemical Society: Washington, DC, 2005.
- (6) Huddleston, J. G.; Visser, A. E.; Reichert, W. M.; Willauer, H. D.; Broker, G. A.; Rogers, R. D. *Green Chem.* **2001**, *3*, 156.
- (7) Brennecke, J. F.; Maginn, E. J. *AIChE J.* **2001**, *47*, 2384.
- (8) Stracke, M. P.; Ebeling, G.; Cataluña, R.; Dupont, J. *Energy Fuels* **2007**, *21*, 1695.
- (9) Moens, L.; Blake, D. M.; Rudnicki, D. L.; Hale, M. J. *J. Sol. Energy Eng.* **2003**, *125*, 112.
- (10) Cocalia, V. A.; Gutowski, K. E.; Rogers, R. D. *Coord. Chem. Rev.* **2006**, *250*, 755.
- (11) Gan, Q.; Rooney, D.; Xue, M. L.; Thompson, G.; Zou, Y. *J. Membr. Sci.* **2006**, *280*, 948.
- (12) Bosmann, A.; Datsevich, L.; Jess, A.; Lauter, A.; Schmitz, C.; Wasserscheid, P. *Chem. Commun.* **2001**, 2494–2495.
- (13) Earle, M.; Seddon, K. *Clean Solvents* **2002**, *819*, 10–25.
- (14) Liu, D.; Gui, J.; Song, L.; Zhang, X.; Sun, Z. *Pet. Sci. Technol.* **2008**, *26*, 973–982.
- (15) Zhang, H.; Wu, J.; Zhang, J.; He, J. *Macromolecules* **2005**, *38*, 8272–8277.
- (16) Barthel, S.; Heinze, T. *Green Chem.* **2006**, *8*, 301.
- (17) Xie, H. L.; Shi, T. J. *Holzforschung* **2006**, *60*, 509.
- (18) Fukaya, Y.; Hayashi, K.; Wada, M.; Ohno, H. *Green Chem.* **2008**, *10*, 44.
- (19) Zhao, H.; Baker, G. A.; Song, Z.; Olubajo, O.; Crittle, T.; Peters, D. *Green Chem.* **2008**, *10*, 696.
- (20) Kazarian, S. G.; Briscoe, B. J.; Welton, T. *Chem. Commun.* **2000**, 2047.
- (21) Aki, S. N. V. K.; Brennecke, J.; Samanta, A. *Chem. Commun.* **2001**, 413.
- (22) Tran, C. D.; De Paoli, L.; Silvia, H.; Oliveira, D. *Appl. Spectrosc.* **2003**, *57*, 152.
- (23) Cammarata, L.; Kazarian, S. G.; Salter, P. A.; Welton, T. *Phys. Chem. Chem. Phys.* **2001**, *3*, 5192–5200.
- (24) Seddon, K. R.; Stark, A.; Torres, M. J. *Pure Appl. Chem.* **2000**, *72*, 2275.
- (25) Liu, H.; Sale, K. L.; Simmons, B. A.; Singh, S. J. *Phys. Chem. B* **2011**, *115*, 10251–10258.
- (26) Mele, A.; Tran, C. D.; Lacerda, S. H. D. A. *Angew. Chem., Int. Ed.* **2003**, *42*, 4364.
- (27) Danten, Y.; Cabaco, M. I.; Besnard, M. *J. Mol. Liq.* **2010**, *153*, 57.
- (28) Xu, Y. J.; Gao, Y.; Zhang, L. Q.; Yao, J.; Wang, C. M.; Li, H. R. *Sci. China, Ser. B: Chem.* **2010**, *53*, 1561.
- (29) Hall, C. A.; Le, K. A.; Rudaz, C.; Radhi, A.; Lovell, C. S.; Damion, R. A.; Budtova, T.; Ries, M. E. J. *Phys. Chem. B* **2012**, *116*, 12810–12818.
- (30) Jiang, W.; Wang, Y.; Voth, G. A. *J. Phys. Chem. B* **2007**, *111*, 4812.
- (31) Canongia Lopes, J. N. A.; Padua, A. A. H. *J. Phys. Chem. B* **2006**, *110*, 3330–3335.
- (32) Klähn, M.; Stüber, C.; Seduraman, A.; Wu, P. *J. Phys. Chem. B* **2010**, *114*, 2856.
- (33) Hanke, C.; Lynden-Bell, R. *J. Phys. Chem. B* **2003**, *107*, 10873–10878.
- (34) Lynden-Bell, R. M.; del Popolo, M. G.; Youngs, T. G. A.; Kohanoff, J.; Hanke, C. G.; Harper, J. B.; Pinilla, C. C. *Acc. Chem. Res.* **2007**, *40*, 1138–1145.
- (35) Liu, H.; Sale, K. L.; Holmes, B. M.; Simmons, B. A.; Singh, S. J. *Phys. Chem. B* **2010**, *114*, 4293–4301.
- (36) Shen, T.; Langan, P.; French, A.; Johnson, S.; Gnanakaran, G. P. *J. Am. Chem. Soc.* **2009**, *131*, 14786.
- (37) del Popolo, M. G.; Voth, G. A. *J. Phys. Chem. B* **2004**, *108*, 1744–1752.
- (38) Kowsari, M. H.; Alavi, S.; Ashrafizadeh, M.; Najafi, B. *J. Chem. Phys.* **2008**, *129*, 224508.
- (39) Raabe, G.; Koehler, J. *J. Chem. Phys.* **2008**, *129*.
- (40) Kahlen, J.; Masuch, K.; Leonhard, K. *Green Chem.* **2010**, *12*, 2172–2181.
- (41) Kirschner, K. N.; Woods, R. J. *Proc. Natl. Acad. Sci. U.S.A.* **2001**, *98*, 10541.
- (42) Feng, S.; Voth, G. A. *Fluid Phase Equilib.* **2010**, *294*, 148–156.
- (43) Viell, J.; Marquardt, W. *Holzforschung* **2011**, *65*, 519–525.
- (44) Plimpton, S. *J. Comput. Phys.* **1995**, *117*, 1–19.
- (45) Canongia Lopes, J. N.; Deschamps, J.; Padua, A. A. H. *J. Phys. Chem. B* **2004**, *108*, 2038–2047.
- (46) Jorgensen, W.; Maxwell, D.; Tirado-Rives, J. *J. Am. Chem. Soc.* **1996**, *118*, 11225–11236.
- (47) Jorgensen, W.; Chandrasekhar, J.; Madura, J.; Impey, R.; Klein, M. *J. Chem. Phys.* **1983**, *79*, 926.
- (48) Ryckaert, J. P.; Ciccotti, G.; Berendsen, H. J. C. *J. Comput. Phys.* **1977**, *23*, 327.
- (49) Hockney, R. W.; Eastwood, J. W. *Computer Simulation Using Particles*; Adam Hilger-IOP: Bristol, UK, 1988.
- (50) Abraham, M. A.; Moens, L. *ACS Symp. Ser.* **2002**, *819*.
- (51) Blanchard, L. A.; Gu, Z.; Brennecke, J. F. *J. Phys. Chem. B* **2001**, *105*, 2437–2444.
- (52) Kelkar, M. S.; Shi, W.; Maginn, E. J. *J. Phys. Chem. B* **2007**, *111*, 4867–4876.
- (53) Haughney, M.; Ferrario, M.; McDonald, I. R. *J. Phys. Chem.* **1987**, *91*, 4934–4940.
- (54) Hess, B.; Kutzner, C.; Spoel, D. V. D.; Lindhal, E. *J. Chem. Theory Comput.* **2008**, *4*.

- (55) Qiao, B.; Krekeler, C.; Berger, R.; Delle Site, L.; Holm, C. *J. Phys. Chem. B* **2008**, *112*, 1743–1751.
- (56) Takamuku, T.; Kyoshoin, Y.; Shimomura, T.; Kittaka, S.; Yamaguchi, T. *J. Phys. Chem. B* **2009**, *113*, 10817–10824.
- (57) Bernardes, C. E. S.; Minas da Piedade, M. E.; Canongia Lopes, J. *N. J. Phys. Chem. B* **2011**, *115*, 2067–2074.
- (58) Méndez-Morales, T.; Carrete, J.; Cabeza, O.; Gallego, L. J.; Varela, L. M. *J. Phys. Chem. B* **2011**, *115*, 6995–7008.
- (59) Méndez-Morales, T.; Carrete, J.; García, M.; Cabeza, O.; Gallego, L. J.; Varela, L. M. *J. Phys. Chem. B* **2011**, *115*, 15313–15322.
- (60) Morrow, T.; Maginn, E. J. *J. Phys. Chem. B* **2002**, *106*, 12807–12813.
- (61) Erdmenger, T.; Haensch, C.; Hoogenboom, R.; Schubert, U. S. *Macromol. Biosci.* **2007**, *7*, 440–445.